

# Enhancement of thermal spin pumping by orbital angular momentum of rare earth iron garnet<sup>★</sup>

Adam B. Cahaya<sup>a,\*,1</sup>

<sup>a</sup>Department of Physics, Faculty of Mathematics and Natural Sciences, Universitas Indonesia, Depok 16424, Indonesia

## ARTICLE INFO

**Keywords:**  
spin pumping  
spin Seebeck effect  
rare earth iron garnet

## ABSTRACT

In a bilayer of ferromagnetic and non-magnetic metal, spin pumping can be generated by a thermal gradient. The spin current generation depends on the spin mixing conductance of the interface and the magnetic properties of the ferromagnetic layer. Due to its low intrinsic damping, rare earth iron garnet is often used for the ferromagnetic layer in the spin Seebeck experiment. However, it is actually a ferrimagnetic with antiferromagnetically coupled magnetic lattices and the contribution of rare earth magnetic lattice of rare earth iron garnet on thermal spin pumping is not well understood. Here we focus on the effect of magnetic properties of lanthanide and show that the orbital angular momentum of rare earth iron garnet enhances thermal spin current generation of lanthanide substituted yttrium iron garnet.

## 1. Introduction

The increased Ohmic losses that are associated with decreasing size of integrated circuits is expected to the breakdown of Moore's law [1]. By employing spin degree of freedom to existing technologies, such as thermoelectric device, the manipulation of spin current alongside electric current can lead to a better efficiency and delay the breakdown[2]. The generation of a pure spin current with no charge current also widely research because it is expected to have less Ohmic loss [3]. At a magnetic interface, a spin current can be generated by electric field [4, 5], ferromagnetic resonance [6, 7] or thermal gradient [8, 9].

One of the mechanism of the spin current generation at an interface of ferromagnet and non-magnetic metal is spin Seebeck effect [10]. The magnitude of the spin current[11]

$$J_s = \frac{\hbar\gamma g^{\uparrow\downarrow}}{2\pi M_s V_c} \Delta T \quad (1)$$

is proportional to temperature different  $\Delta T$  across the interface, spin mixing conductance  $g^{\uparrow\downarrow}$  of the interface [12], gyromagnetic ratio  $\gamma$  and the inverse of the saturated magnetization  $M_s$  of the ferromagnetic layer.  $V_c$  is the magnetic coherence volume of the magnetic layer [13]. At the ferromagnet side, the spin angular momentum loss can be detected as enhancement in the magnetic damping. At the non-magnetic metal side, the spin current can be detected as an electric voltage by means of the inverse spin Hall effect [5]. The direction of the detected electric current is perpendicular to both spin current direction and magnetization of the ferromagnet.

Thermal spin pumping can also occurs when the magnetic layer is antiferromagnetic, such as  $\text{MnFe}_2$ [14, 15] or a ferrimagnetic insulator such as  $\text{Y}_3\text{Fe}_5\text{O}_{12}$  (YIG) [16, 17]. Furthermore, transition near the magnetization compensation point of  $\text{Gd}_3\text{Fe}_5\text{O}_{12}$  is observed as the switch of the polarization of the generated spin current [18, 19]. Recently, it has been observed that spin Seebeck effect can be enhanced by substituting yttrium in ferrimagnetic YIG by rare earths [20, 21]. While machine-learning has been employed for optimizing the spin Seebeck effect[21], a deeper physical understanding on the role of lanthanide on thermal spin pumping is

required.

In this article, we investigate the role of lanthanide magnetic moment in the thermal spin pumping of lanthanide substituted YIG,  $\text{RY}_2\text{Fe}_5\text{O}_{12}$ . Sec. 2 describes thermal spin pumping from ferrimagnet with two magnetic sublattice. Sec. 3 discuss the coupling of Fe and Lanthanide (R) magnetic lattices and its effect on  $V_c$ ,  $M_s$  and  $\gamma$ . While  $M_s$  and  $\gamma$  of rare earth iron garnet is widely studied, their combined relation to thermal spin pumping are not so well described. We analyze the effect of R angular momentum on  $g^{\uparrow\downarrow}$  and the resultant spin current in Sec. 4 and summarize the thermal spinning of  $\text{RY}_2\text{Fe}_5\text{O}_{12}|\text{Pt}$  in Sec. 5.

## 2. Thermal spin pumping from ferrimagnet

Ref. [11] derived Eq. 1 for describing spin Seebeck effect from ferromagnet to non-magnetic metal. Thermally generated spin current arises from spin pumping from ferromagnetic layer to non-magnetic layer [25]

$$\mathbf{J}_{sp} = g^{\uparrow\downarrow} \mathbf{m} \times \dot{\mathbf{m}}, \quad (2)$$

and backflow spin current due to Johnson Nyquist thermal noise.

$$\mathbf{J}_m = M_s V_c \dot{\mathbf{m}} \times \mathbf{h}. \quad (3)$$

Here  $\mathbf{m}$  is magnetization direction,  $\mathbf{h}$  is zero-averaged magnetic field noise [26]

$$\langle h_i(t) h_j(t') \rangle = \frac{2k_B T \alpha}{\gamma M_s V_c} \delta_{ij} \delta(t - t'), \quad (4)$$

$\alpha$  is damping constant. At the magnetic interface  $\alpha$  dominantly arise from the spin mixing at the interface and the averaged spin current is proportional to the temperature difference across the interface[11]

$$J_s = \langle g^{\uparrow\downarrow} \mathbf{m} \times \dot{\mathbf{m}} + M_s V_c \dot{\mathbf{m}} \times \mathbf{h} \rangle = \frac{\hbar\gamma g^{\uparrow\downarrow}}{2\pi M_s V_c} \Delta T. \quad (5)$$

While the spin pumping of  $\text{Y}_3\text{Fe}_5\text{O}_{12}$  can be described by the dynamic of Fe magnetic moment alone [27], the total spin current generation of  $\text{RY}_2\text{Fe}_5\text{O}_{12}$  require two magnetic sub-lattices model. Since the spin mixing conductance is shown to arise from the exchange interaction between the localized spin of ferromagnet and conduction spin of the non-magnetic metal [27, 28, 29]

$$g^{\uparrow\downarrow} \propto J_{\text{ex}}^2 (S_{\text{Fe}} - |g_J - 1| J_{\text{R}})^2, \quad (6)$$

<sup>★</sup>This document is supported by Universitas Indonesia via Grant PUTI No. NKB-995/UN2.RST/HKP.05.00/2020

✉ adam@sci.ui.ac.id (A.B. Cahaya)  
ORCID(s): 0000-0002-2068-9613 (A.B. Cahaya)

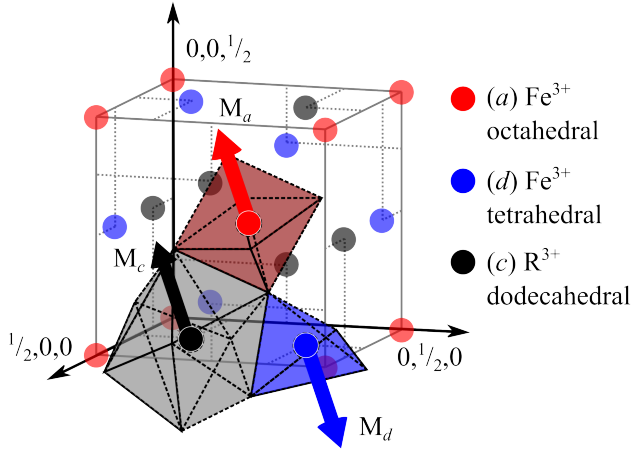


**Figure 1:** One eighth of a unit cell of  $R_3Fe_5O_{12}$  [22, 23]. The garnet structure has metal cations ( $Fe^{3+}$  and  $R^{3+}$ ) and oxygen anions that form tetrahedral ( $a$ ), octahedral ( $d$ ) and dodecahedral ( $c$ ) sites [24].  $a$  and  $d$  sites are occupied by  $Fe^{3+}$ .  $c$ -site is occupied by  $Y^{3+}$  or trivalent lanthanide elements (denoted by  $R^{3+}$ ).  $c$  and  $a$  sites are coupled antiferromagnetically with  $d$ -site.

where  $S_{Fe}$  and  $|g_J - 1|J_R$  are spin of iron and lanthanide (R) magnetic sublattices, respectively.  $J_{ex}$  is the exchange constant between the localized spin of rare earth iron garnet and conduction spin of the non-magnetic metal, which mainly depend on the non-magnetic metal when the ferromagnet is an insulator, such as rare earth iron garnets [30].

### 3. Coupled dynamics of rare earth iron garnet

The magnetization of rare earth garnet arises from the magnetic moments of trivalent ions of iron and lanthanide (R). As seen in Fig. 1,  $Fe^{3+}$  occupies tetrahedral ( $d$ ) and octahedral ( $a$ ) site, while  $R^{3+}$  occupy dodecahedral ( $c$ ) site [24]. Since  $a$  and  $c$  sites are antiferromagnetically coupled to  $d$ -site, the total magnetization of  $RY_2Fe_5O_{12}$  are

$$M_s = M_{Fe} - M_R. \quad (7)$$

For  $x = 1$ , the magnetization of  $RY_2Fe_5O_{12}$  can be determined using two sub lattice model of Fe and R [31].

While demagnetizing fields and crystallographic anisotropy may affect spin current generations, in this article we will focus on the effect of the exchange coupling of magnetic lattices. The exchange coupling can be written using interaction Hamiltonian consists of ferromagnetic coupling between Fe spins of neighboring lattice and antiferromagnetic coupling between R and Fe spins at the same lattice

$$H_{int} = \lambda \sum_n |g_J - 1| \mathbf{J}_R^n \cdot \mathbf{S}_{Fe}^n - I \sum_n \mathbf{S}_{Fe}^n \cdot \mathbf{S}_{Fe}^{n+1}. \quad (8)$$

Here  $\mathbf{S}_{Fe}^n = \mathbf{M}_{Fe}/(2\gamma_0)$  and  $\mathbf{J}_R^n = \mathbf{M}_R/(g_J\gamma_0)$  are angular momentums of Fe and R at  $n$ -th site, respectively.  $g_J$  is Lande  $g$ -factor.  $I$  and  $\lambda$  are the exchange constants that depends on the distances between spins.

The Landau–Lifshitz equations of the spins under magnetic field  $\mathbf{H}$  are

$$\frac{d\mathbf{S}_{Fe}^n}{dt} = \mathbf{S}_{Fe}^n \times \left( 2\gamma_0\mathbf{H} + I \sum_{m=n\pm 1} \mathbf{S}_{Fe}^m - |g_J - 1| \mathbf{J}_R \right),$$

$$\frac{d\mathbf{J}_R^n}{dt} = \mathbf{J}_R^n \times (g_J\gamma_0\mathbf{H} - |g_J - 1|\lambda\mathbf{S}_{Fe}^n). \quad (9)$$

where  $\gamma_0$  is the classical gyromagnetic ratio. The coupled equations can be linearized by setting  $F_{\pm}^n = F_x^n \pm iF_y^n = F_{\pm}^n e^{i(nk \cdot a - \omega t)}$ .

$$\frac{d}{dt} \begin{bmatrix} S_{Fe}^+ \\ J_R^+ \end{bmatrix} = iW \begin{bmatrix} S_{Fe}^+ \\ J_R^+ \end{bmatrix}, \quad (10)$$

$$W = \begin{bmatrix} 2\gamma_0 H - 4IS_{Fe} \sin^2 \frac{ka}{2} + |g_J - 1|\lambda J_R & |g_J - 1|\lambda S_{Fe} \\ -|g_J - 1|\lambda J_R & g_J\gamma_0 H - |g_J - 1|\lambda S_{Fe} \end{bmatrix}.$$

The eigenvalues of the matrix is

$$\omega_{1,2} = \frac{4I \sin^2 \frac{ka}{2} - \lambda'(S_{Fe} - J_R) + (S_{Fe} - J_R)H}{2} \left( 1 \pm \sqrt{1 + 4 \frac{(\lambda' S_{Fe} - g_J \gamma_0 H)(4I \sin^2 \frac{ka}{2} + \lambda' J_R + 2\gamma_0 H) + 4\lambda'^2 J_R S_{Fe}}{(4I \sin^2 \frac{ka}{2} - \lambda'(S_{Fe} - J_R) + (S_{Fe} - J_R)H)^2}} \right), \quad (11)$$

where  $\lambda' = |g_J - 1|\lambda$ . here  $a$  and  $k$  are lattice constant and wave vector. Two limits,  $k = 0$  ( $H \neq 0$ ) and  $H = 0$  ( $k \neq 0$ ) are useful for analyzing the effect of rare earth magnetic sub-lattice on  $V_c$ ,  $M_s$  and  $\gamma$ .

#### 3.1. Magnetic moment of lanthanide sublattice

The spin wave modes in Fig. 2 can be found from eigenfrequencies of matrix in Eq. 11 for  $H = 0$ ,

$$\omega_1(H = 0) = 4IS_{Fe} \sin^2 \frac{ka}{2} + |g_J - 1|\lambda J_R \quad (12)$$

$$\omega_2(H = 0) = -|g_J - 1|\lambda S_{Fe} \quad (13)$$

for  $IS_{Fe} \gg \lambda(S_{Fe} - J_R)$ . Eq. 12 indicates that the changes of the spin wave stiffness

$$D = \lim_{ka \ll 1} \frac{1}{2} \frac{\partial^2 \omega_1}{\partial k^2} \simeq IS_{Fe} a^2 \quad (14)$$

due to rare earth sublattice only depends on the change of lattice constant. The effects of spin wave on the spin current generation is widely researched [32, 33, 34] and the effect of the spin wave on thermal spin pumping is captured on magnetic coherence volume  $V_c$ , which is directly related to the spin wave stiffness [13]

$$V_c \propto D^{3/2} \propto a^3. \quad (15)$$

While lattice constants of  $R_3Fe_5O_{12}$  is well studied [35], in this article we will assume that the changes of  $a$  due to small R substitution  $RY_2Fe_5O_{12}$ , which is less than 1% [36], is negligible.

Eq. 13 indicates that rare earth magnetic sub-lattice of rare earth iron garnet gives an optical branch on its spin wave dispersion [31]. The optical spin wave mode  $\omega_2$  can be associated with the paramagnetic response of R to Fe molecular field. The temperature dependence of  $M_R = g_J J_R$  with quantum number of total angular momentum  $J$  can be determined from the statistical averaged of  $J_R$

$$\begin{aligned} J_R(T) &= \left( \sum_{J_z} J_z e^{-\omega_2 J_z / k_B T} \right) / \left( \sum_{J_z} e^{-\omega_2 J_z / k_B T} \right) \\ &= J B_J \left( \frac{|g_J - 1|\lambda S_{Fe}}{k_B T} \right), \end{aligned} \quad (16)$$

$B_J$  is the Brillouin function. Since  $\lim_{x \rightarrow 0} B_J(x) = (J + 1)x/3$ ,  $M_R$  at a high temperature can be approximated using Curie law

$$J_R(T) = \frac{|g_J - 1|J(J + 1)\lambda S_{Fe}}{3k_B T}. \quad (17)$$

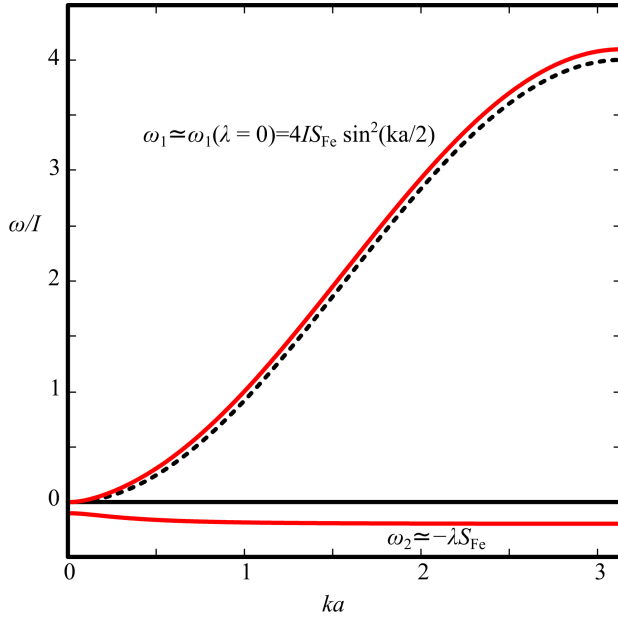


**Figure 2:** Spin-wave spectra of two-sublattice models of  $\text{RY}_2\text{Fe}_5\text{O}_{12}$  (red lines). The spectrum of ferromagnetic spin wave  $\omega_1$  of iron chain with spin  $S_{\text{Fe}}$  is approximately the same as the unperturbed one (black dashed line). The antiferromagnetic coupling between Fe and R generate an optical branch  $\omega_2 = -\lambda S_{\text{Fe}}$ ,  $\lambda$  is exchange constant of Fe and R.

The sign switching of  $M_s = 2S_{\text{Fe}} - xg_J J_{\text{R}}$  happen at compensation point [24, 37]

$$T_{\text{comp}} = \frac{x\lambda g_J |g_J - 1| J(J+1)}{6k_B}. \quad (18)$$

The sign switching of  $M$  near compensation point is observed as a switching of the spin polarization of the spin current [18, 19]. Fig. 3 illustrate the relation in Eq. 18 for

$$\lambda = \begin{cases} \lambda_1 = 2.78 \times 10^{-2} k_B T_C, \\ \lambda_2 = (8.2 + 0.7g_J |g_J - 1| J(J+1)) \times 10^{-2} k_B T_C, \end{cases} \quad (19)$$

obtained from linear and parabolic fitting of  $T_{\text{comp}}$  to experimental data from Ref. [24].

### 3.2. Gyromagnetic ratio

Gyromagnetic ratio  $\gamma$  of  $\text{RY}_2\text{Fe}_5\text{O}_{12}$  can be determined by considering  $k = 0$  with  $\mathbf{H} \neq 0$  limit of Eq. 11

$$\omega_1(k=0) = |g_J - 1| \lambda (J_{\text{R}} - S_{\text{Fe}}) + \mathcal{O}(H), \quad (20)$$

$$\omega_2(k=0) = \gamma_0 H \frac{2S_{\text{Fe}} - g_J J_{\text{R}}}{S_{\text{Fe}} - J_{\text{R}}} + \mathcal{O}(H^2). \quad (21)$$

Eq. 20 is related to Kaplan–Kittel frequency of two-sublattice system [35, 38] in THz regime [39]. The resultant gyromagnetic ratio can be obtained from the lower eigenvalue (Eq. 21)

$$\gamma = \left[ \frac{\partial \omega_2(k=0)}{\partial H} \right]_{H=0} = \gamma_0 \frac{2S_{\text{Fe}} - g_J J_{\text{R}}}{S_{\text{Fe}} - J_{\text{R}}}. \quad (22)$$

Since orbital angular momentum is  $L = (2 - g_J)J$ , one can see orbital angular momentum increase  $\gamma$  of the rare earth element

$$\lim_{J_{\text{R}} \ll S_{\text{Fe}}} \gamma \approx 2\gamma_0 \left( 1 + \frac{2-g_J}{2} \frac{J_{\text{R}}}{S_{\text{Fe}}} \right) = 2\gamma_0 \left( 1 + \frac{L_{\text{R}}}{2S_{\text{Fe}}} \right). \quad (23)$$

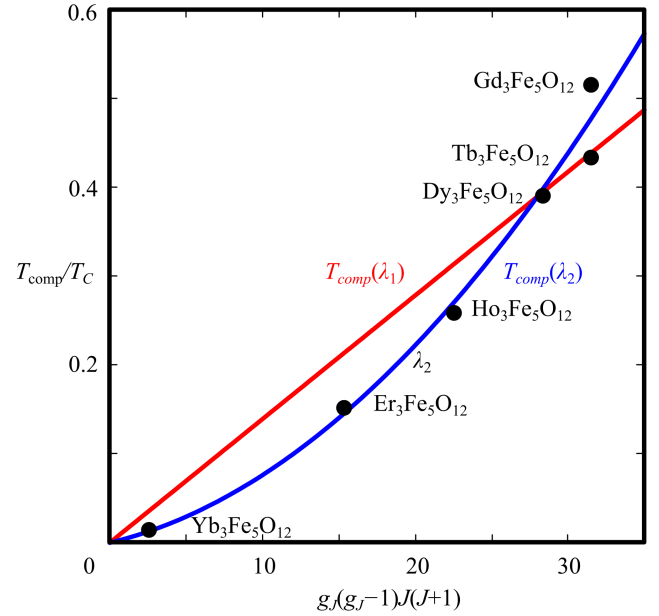


**Figure 3:** Compensation temperature  $T_{\text{comp}}$  of  $\text{R}_3\text{Fe}_5\text{O}_{12}$  is proportional to  $\lambda g_J |g_J - 1| J(J+1)$ . The red line corresponds to  $\lambda_1 = 2.78 \times 10^{-2} k_B T_C$ , obtained from linear fitting to experiment data from Ref. [24]. The blue line corresponds to  $\lambda_2 = (8.2 + 0.7g_J |g_J - 1| J(J+1)) \times 10^{-3} k_B T_C$  obtained from parabolic fitting for better agreement.  $T_C$  is the Curie temperature. At the compensation temperature total magnetization  $M_s = M_{\text{Fe}} - M_{\text{R}}$  changes sign.

## 4. Enhanced spin current generation

By combining the influence of lanthanide on  $V_c$ ,  $M_s$ ,  $\gamma$  and  $g^{1\downarrow}$ , we can arrive at the following proportionality

$$J_s \propto \frac{(S_{\text{Fe}} - |g_J - 1| J_{\text{R}})^2}{S_{\text{Fe}} - J_{\text{R}}} \quad (24)$$

For heavier lanthanide  $g_J > 1$ , one can see that the spin current is enhanced by orbital angular momentum

$$\lim_{J_{\text{R}} \ll S_{\text{Fe}}} J_s \propto \left( 1 + \frac{(3 - 2g_J)J_{\text{R}}}{S_{\text{Fe}}} \right) = \left( 1 + \frac{L_{\text{R}} - S_{\text{R}}}{S_{\text{Fe}}} \right) \quad (25)$$

Here,  $L_{\text{R}}$  and  $S_{\text{R}}$  are coupled to  $J_{\text{R}}$ , which expectation value is described in Eq. 17. Fig. 4 illustrates the values of thermal spin pumping of  $\text{RY}_2\text{Fe}_5\text{O}_{12}|\text{Pt}$  compared to those of  $\text{Y}_3\text{Fe}_5\text{O}_{12}|\text{Pt}$  in room temperature  $T \sim 0.5T_C$  and shows the agreement to experiment data by Ref. [21].

The larger value of  $\text{LuY}_2\text{Fe}_5\text{O}_{12}$  compared to  $\text{LaY}_2\text{Fe}_5\text{O}_{12}$  may come from the decrease of rare earth garnet lattice constant. The decreasing value may also rise from the low heat conductance of YIG, which reduces temperature different at the interface [12]. By adding a corrected exchange constant ( $\lambda_2$ ) obtained from parabolic fitting in Fig. 3, the resultant thermal spin pumping agrees with the values for heavy end of lanthanide series.

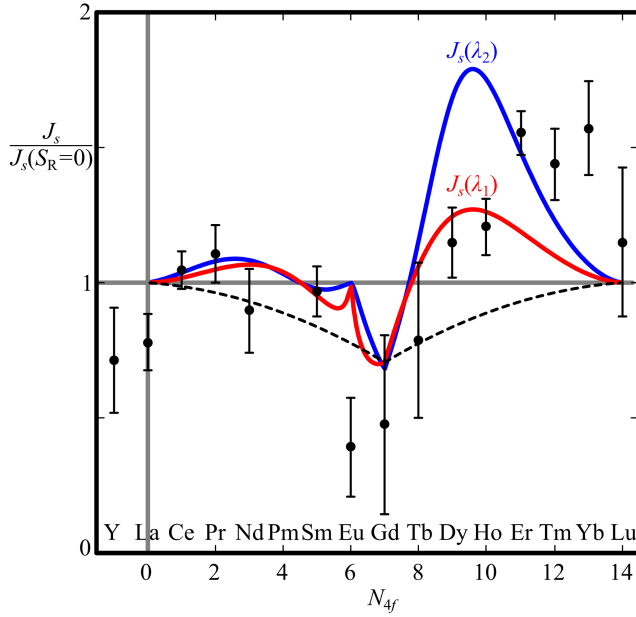


**Figure 4:** Spin current generated by thermal spin pumping in  $\text{RY}_2\text{Fe}_5\text{O}_{12}|\text{Pt}$  bilayer. The spin current can be enhanced by substituting one of yttriums with a lanthanide element. The experimental data was taken from spin Seebeck effect of substituted  $\text{Y}_3\text{Fe}_5\text{O}_{12}|\text{Pt}$  from Ref. [21], tabulated in Table 1. The value is normalized to the averaged value of  $\text{LaY}_2\text{Fe}_5\text{O}_{12}$  and  $\text{LuY}_2\text{Fe}_5\text{O}_{12}$ . Red and blue lines show the values for exchange constant  $\lambda_1$  and  $\lambda_2$ , respectively. The former captures the general trends of the spin current enhancement. The correction of  $\lambda_2$  from parabolic fitting in Fig. 2 matches the values of  $\text{ErY}_2\text{Fe}_5\text{O}_{12}$  and  $\text{TmY}_2\text{Fe}_5\text{O}_{12}$ . Dashed black line shows the values when the spin-orbit coupling of rare earth is weak and only the spin angular momentums contributes to the magnetization and thermal spin pumping.

## 5. Conclusion

To summarize, we consider two magnetic sub-lattice model for describing the thermal spin pumping of rare earth iron garnet. The effect of lanthanide magnetic moment on the thermal spin pumping of rare earth iron garnet arise from its contribution on  $M_s$ ,  $\gamma$  and  $g^{\uparrow\downarrow}$ . While the angular momentum of R does not affect  $V_c$  and reduces  $g^{\uparrow\downarrow}$ , it enhances the thermal spin pumping by reducing  $M_s$  and increasing  $\gamma$ .

Magnetic moment of lanthanide is paramagnetically response to the molecular field of Fe. Generally, the exchange coupling constant between Fe and R can be assumed constant ( $\lambda = \lambda_1$ ) for all lanthanide elements. A correction factor may be added from parabolic fitting in Fig. 3. The resultant thermal spin pumping agrees with the values for heavy end of lanthanide series. The maximum value of thermal spin pumping is achieved when the difference between orbital and spin angular momentum of the rare earth is maximum.

The deviation between theoretical and experimental values may arise from the dependency of crystalline and interface parameters to the lanthanide substitution, such as lattice parameter,  $g$ -factor and crystalline anisotropy. The present modeling is also applicable for other ferrimagnetic materials.

**Table 1**

Voltage ( $\mu\text{V}/\text{K}$ ) generated from spin Seebeck effect, which is proportional to the thermally generated spin current in Eq. 1. The tabulated data is extracted from Ref. [21].  $\text{RY}_2\text{Fe}_5\text{O}_{12}|\text{Pt}$  was grown in two kinds of substrates:  $\text{Gd}_3\text{Ga}_5\text{O}_{12}$  (GGG) and  $\text{Gd}_{2.675}\text{Ca}_{0.325}\text{Ga}_{4.025}\text{Mg}_{0.325}\text{Zr}_{0.65}\text{O}_{12}$  (SGGG). The spin Seebeck voltage of YIG is set to  $2.46 \mu\text{V}/\text{K}$ .

R	GGG	SGGG	weighted averaged
Y	$2.46 \pm 0.09$	$1.32 \pm 0.24$	$2.14 \pm 0.58$
La	$2.23 \pm 0.59$	$2.36 \pm 0.10$	$2.34 \pm 0.31$
Ce	$3.09 \pm 0.36$	$3.17 \pm 0.19$	$3.14 \pm 0.21$
Pr	$2.89 \pm 0.18$	$3.51 \pm 0.08$	$3.32 \pm 0.32$
Nd	$2.09 \pm 0.29$	$2.96 \pm 0.12$	$2.69 \pm 0.46$
Sm	$3.23 \pm 0.18$	$2.71 \pm 0.10$	$2.90 \pm 0.28$
Eu	$1.72 \pm 0.14$	$0.65 \pm 0.13$	$1.18 \pm 0.55$
Gd	$2.70 \pm 0.15$	$0.72 \pm 0.09$	$1.43 \pm 0.99$
Tb	$2.74 \pm 0.10$	$1.04 \pm 0.34$	$2.36 \pm 0.86$
Dy	$3.87 \pm 0.31$	$3.17 \pm 0.19$	$3.44 \pm 0.39$
Ho	$3.92 \pm 0.09$	$3.31 \pm 0.09$	$3.62 \pm 0.31$
Er	$4.77 \pm 0.20$	$4.48 \pm 0.33$	$4.66 \pm 0.24$
Tm	$4.54 \pm 0.12$	$3.81 \pm 0.24$	$4.31 \pm 0.39$
Yb	$5.35 \pm 0.30$	$4.37 \pm 0.16$	$4.71 \pm 0.52$
Lu	$3.91 \pm 0.05$	$2.27 \pm 0.13$	$3.45 \pm 0.82$

## Declaration of competing interest

The authors declare that they have no known competing financial interests or personal relationships that could have appeared to influence the work reported in this paper.

## References

- [1] C. H. Marrows, B. J. Hickey, New directions in spintronics, *Philosophical Transactions of the Royal Society A: Mathematical, Physical and Engineering Sciences* 369 (2011) 3027–3036. URL: <https://doi.org/10.1098/rsta.2011.0156>. doi:10.1098/rsta.2011.0156.
- [2] J. Linder, M. E. Bathen, Spin caloritronics with superconductors: Enhanced thermoelectric effects, generalized Onsager response-matrix, and thermal spin currents, *Phys. Rev. B* 93 (2016) 224509. URL: <https://link.aps.org/doi/10.1103/PhysRevB.93.224509>. doi:10.1103/PhysRevB.93.224509.
- [3] S. R. Bakaul, S. Hu, T. Kimura, Large pure spin current generation in metallic nanostructures, *Applied Physics A* 111 (2012) 355–360. URL: <https://doi.org/10.1007/s00339-012-7495-0>. doi:10.1007/s00339-012-7495-0.
- [4] J. Sinova, S. O. Valenzuela, J. Wunderlich, C. H. Back, T. Jungwirth, Spin Hall effects, *Rev. Mod. Phys.* 87 (2015) 1213–1260. URL: <https://link.aps.org/doi/10.1103/RevModPhys.87.1213>. doi:10.1103/RevModPhys.87.1213.
- [5] S. Takahashi, S. Maekawa, Spin current, spin accumulation and spin Hall effect, *Science and Technology of Advanced Materials* 9 (2008) 014105. URL: <https://doi.org/10.1088/1468-6996/9/1/014105>. doi:10.1088/1468-6996/9/1/014105.
- [6] S. Mizukami, Y. Ando, T. Miyazaki, The study on ferromagnetic resonance linewidth for NM/80nife/NM (NM=Cu, Ta, Pd and Pt) films, *Japanese Journal of Applied Physics* 40 (2001) 580–585. URL: <https://doi.org/10.1143/jjap.40.580>. doi:10.1143/jjap.40.580.



- [7] R. Urban, G. Woltersdorf, B. Heinrich, Gilbert damping in single and multilayer ultrathin films: Role of interfaces in nonlocal spin dynamics, *Phys. Rev. Lett.* 87 (2001) 217204. URL: <https://link.aps.org/doi/10.1103/PhysRevLett.87.217204>. doi:10.1103/PhysRevLett.87.217204.
- [8] K. Uchida, S. Takahashi, K. Harii, J. Ieda, W. Koshibae, K. Ando, S. Maekawa, E. Saitoh, Observation of the spin Seebeck effect, *Nature* 455 (2008) 778–781. URL: <https://doi.org/10.1038/nature07321>. doi:10.1038/nature07321.
- [9] A. B. Cahaya, A. O. Tretiakov, G. E. W. Bauer, Spin Seebeck power conversion, *IEEE Transactions on Magnetics* 51 (2015) 1–14. doi:10.1109/TMAG.2015.2436362.
- [10] G. E. W. Bauer, E. Saitoh, B. J. van Wees, Spin caloritronics, *Nature Materials* 11 (2012) 391–399. URL: <https://doi.org/10.1038/nmat3301>. doi:10.1038/nmat3301.
- [11] J. Xiao, G. E. W. Bauer, K.-c. Uchida, E. Saitoh, S. Maekawa, Theory of magnon-driven spin Seebeck effect, *Phys. Rev. B* 81 (2010) 214418. URL: <https://link.aps.org/doi/10.1103/PhysRevB.81.214418>. doi:10.1103/PhysRevB.81.214418.
- [12] M. Weiler, M. Althammer, M. Schreier, J. Lotze, M. Pernpeintner, S. Meyer, H. Huebl, R. Gross, A. Kamra, J. Xiao, Y.-T. Chen, H. J. Jiao, G. E. W. Bauer, S. T. B. Goennenwein, Experimental test of the spin mixing interface conductivity concept, *Phys. Rev. Lett.* 111 (2013) 176601. URL: <https://link.aps.org/doi/10.1103/PhysRevLett.111.176601>. doi:10.1103/PhysRevLett.111.176601.
- [13] J. Xiao, G. E. W. Bauer, K.-C. Uchida, E. Saitoh, S. Maekawa, Erratum: Theory of magnon-driven spin Seebeck effect [phys. rev. b 81, 214418 (2010)], *Phys. Rev. B* 82 (2010) 099904(E). URL: <https://link.aps.org/doi/10.1103/PhysRevB.82.099904>. doi:10.1103/PhysRevB.82.099904.
- [14] S. M. Wu, W. Zhang, K. Amit, P. Borisov, J. E. Pearson, J. S. Jiang, D. Lederman, A. Hoffmann, A. Bhattacharya, Antiferromagnetic spin Seebeck effect, *Phys. Rev. Lett.* 116 (2016) 097204(B). URL: <https://link.aps.org/doi/10.1103/PhysRevLett.116.097204>. doi:10.1103/PhysRevLett.116.097204.
- [15] S. M. Rezende, R. L. Rodríguez-Suárez, A. Azevedo, Theory of the spin Seebeck effect in antiferromagnets, *Phys. Rev. B* 93 (2016) 014425. URL: <https://link.aps.org/doi/10.1103/PhysRevB.93.014425>. doi:10.1103/PhysRevB.93.014425.
- [16] K. Uchida, J. Xiao, H. Adachi, J. Ohe, S. Takahashi, J. Ieda, T. Ota, Y. Kajiwara, H. Umezawa, H. Kawai, G. E. W. Bauer, S. Maekawa, E. Saitoh, Spin Seebeck insulator, *Nature Materials* 9 (2010) 894–897. URL: <https://doi.org/10.1038/nmat2856>. doi:10.1038/nmat2856.
- [17] K. ichi Uchida, H. Adachi, T. Ota, H. Nakayama, S. Maekawa, E. Saitoh, Observation of longitudinal spin-Seebeck effect in magnetic insulators, *Applied Physics Letters* 97 (2010) 172505. URL: <https://doi.org/10.1063/1.3507386>. doi:10.1063/1.3507386.
- [18] S. Geprägs, A. Kehlberger, F. D. Coletta, Z. Qiu, E.-J. Guo, T. Schulz, C. Mix, S. Meyer, A. Kamra, M. Althammer, H. Huebl, G. Jakob, Y. Ohnuma, H. Adachi, J. Barker, S. Maekawa, G. E. W. Bauer, E. Saitoh, R. Gross, S. T. B. Goennenwein, M. Kläui, Origin of the spin Seebeck effect in compensated ferrimagnets, *Nature Communications* 7 (2016) 10452. URL: <https://doi.org/10.1038/ncomms10452>. doi:10.1038/ncomms10452.
- [19] K. Shen, Temperature-switched anomaly in the spin Seebeck effect in  $\text{gd}_3\text{fe}_5\text{o}_{12}$ , *Phys. Rev. B* 99 (2019) 024417. URL: <https://link.aps.org/doi/10.1103/PhysRevB.99.024417>. doi:10.1103/PhysRevB.99.024417.
- [20] V. H. Ortiz, M. J. Gomez, Y. Liu, M. Aldosary, J. Shi, R. B. Wilson, Ultrafast measurements of the interfacial spin Seebeck effect in au and rare-earth iron-garnet bilayers, *Phys. Rev. Materials* 5 (2021) 074401. URL: <https://link.aps.org/doi/10.1103/PhysRevMaterials.5.074401>. doi:10.1103/PhysRevMaterials.5.074401.
- [21] Y. Iwasaki, I. Takeuchi, V. Stanev, A. G. Kusne, M. Ishida, A. Kirihara, K. Ihara, R. Sawada, K. Terashima, H. Someya, K.-i. Uchida, E. Saitoh, S. Yorozu, Machine-learning guided discovery of a new thermoelectric material, *Scientific Reports* 9 (2019) 2751. URL: <https://doi.org/10.1038/s41598-019-39278-z>. doi:10.1038/s41598-019-39278-z.
- [22] A. Jain, S. P. Ong, G. Hautier, W. Chen, W. D. Richards, S. Dacek, S. Cholia, D. Gunter, D. Skinner, G. Ceder, K. a. Persson, The Materials Project: A materials genome approach to accelerating materials innovation, *APL Materials* 1 (2013) 011002. URL: <http://link.aip.org/link/AMPADS/v1/i1/p011002/s1&Agg=doi>. doi:10.1063/1.4812323.
- [23] K. Momma, F. Izumi, VESTA3 for three-dimensional visualization of crystal, volumetric and morphology data, *Journal of Applied Crystallography* 44 (2011) 1272–1276. URL: <https://doi.org/10.1107/S0021889811038970>. doi:10.1107/S0021889811038970.
- [24] M. Gilleo, Chapter 1 ferromagnetic insulators: Garnets, volume 2 of *Handbook of Ferromagnetic Materials*, Elsevier, 1980, pp. 1–53. URL: <https://www.sciencedirect.com/science/article/pii/S1574930405801026>. doi:https://doi.org/10.1016/S1574-9304(05)80102-6.
- [25] Y. Tserkovnyak, A. Brataas, G. E. W. Bauer, Spin pumping and magnetization dynamics in metallic multilayers, *Phys. Rev. B* 66 (2002) 224403. URL: <https://link.aps.org/doi/10.1103/PhysRevB.66.224403>. doi:10.1103/PhysRevB.66.224403.
- [26] J. Foros, A. Brataas, Y. Tserkovnyak, G. E. W. Bauer, Magnetization noise in magneto-electronic nanostructures, *Phys. Rev. Lett.* 95 (2005) 016601. URL: <https://link.aps.org/doi/10.1103/PhysRevLett.95.016601>. doi:10.1103/PhysRevLett.95.016601.
- [27] A. B. Cahaya, A. O. Leon, G. E. W. Bauer, Crystal field effects on spin pumping, *Phys. Rev. B* 96 (2017) 144434. URL: <https://link.aps.org/doi/10.1103/PhysRevB.96.144434>. doi:10.1103/PhysRevB.96.144434.
- [28] A. B. Cahaya, Antiferromagnetic spin pumping via hyperfine interaction, *Hyperfine Interactions* 242 (2021) 46. URL: <https://doi.org/10.1007/s10751-021-01780-0>. doi:10.1007/s10751-021-01780-0.
- [29] A. B. Cahaya, Adiabatic limit of RKKY range function in one dimension, *Journal of Magnetism and Magnetic Materials* 547 (2022) 168874. URL: <https://www.sciencedirect.com/science/article/pii/S0304885321010805>. doi:https://doi.org/10.1016/j.jmmm.2021.168874.
- [30] A. B. Cahaya, M. A. Majidi, Effects of screened Coulomb interaction on spin transfer torque, *Phys. Rev. B* 103 (2021) 094420. URL: <https://link.aps.org/doi/10.1103/PhysRevB.103.094420>. doi:10.1103/PhysRevB.103.094420.
- [31] M. Tinkham, Low-lying spectrum of rare-earth iron garnets, *Phys. Rev.* 124 (1961) 311–320. URL: <https://link.aps.org/doi/10.1103/PhysRev.124.311>. doi:10.1103/PhysRev.124.311.
- [32] H. Jin, S. R. Boona, Z. Yang, R. C. Myers, J. P. Heremans, Effect of the magnon dispersion on the longitudinal spin Seebeck effect in yttrium iron garnets, *Phys. Rev. B* 92 (2015) 054436. URL: <https://link.aps.org/doi/10.1103/PhysRevB.92.054436>. doi:10.1103/PhysRevB.92.054436.
- [33] A. Prakash, B. Flebus, J. Brangham, F. Yang, Y. Tserkovnyak, J. P. Heremans, Evidence for the role of the magnon energy relaxation length in the spin Seebeck effect, *Phys. Rev. B* 97 (2018) 020408. URL: <https://link.aps.org/doi/10.1103/PhysRevB.97.020408>. doi:10.1103/PhysRevB.97.020408.
- [34] T. Kikkawa, K. Shen, B. Flebus, R. A. Duine, K.-i. Uchida, Z. Qiu, G. E. W. Bauer, E. Saitoh, Magnon polarons in the spin Seebeck effect, *Phys. Rev. Lett.* 117 (2016) 207203. URL: <https://link.aps.org/doi/10.1103/PhysRevLett.117.207203>. doi:10.1103/PhysRevLett.117.207203.
- [35] R. Nakamoto, B. Xu, C. Xu, H. Xu, L. Bellaiche, Properties of rare-earth iron garnets from first principles, *Phys. Rev. B* 95 (2017) 024434. URL: <https://link.aps.org/doi/10.1103/PhysRevB.95.024434>. doi:10.1103/PhysRevB.95.024434.
- [36] G. P. Espinosa, Crystal chemical study of the rare-earth iron garnets, *The Journal of Chemical Physics* 37 (1962) 2344–2347. URL: <https://doi.org/10.1063/1.1733008>. doi:10.1063/1.1733008. arXiv:https://doi.org/10.1063/1.1733008.
- [37] W. P. Wolf, J. H. Van Vleck, Magnetism of europium garnet, *Phys. Rev.* 118 (1960) 1490–1492. URL: <https://link.aps.org/doi/10.1103/PhysRev.118.1490>. doi:10.1103/PhysRev.118.1490.
- [38] J. Kaplan, C. Kittel, Exchange frequency electron spin reso-

nance in ferrites, *The Journal of Chemical Physics* 21 (1953) 760–761. URL: <https://doi.org/10.1063/1.1699018>. doi:10.1063/1.1699018. arXiv:<https://doi.org/10.1063/1.1699018>.

- [39] W.-H. Hsu, K. Shen, Y. Fujii, A. Koreeda, T. Satoh, Observation of terahertz magnon of Kaplan-Kittel exchange resonance in yttrium-iron garnet by raman spectroscopy, *Phys. Rev. B* 102 (2020) 174432. URL: <https://link.aps.org/doi/10.1103/PhysRevB.102.174432>. doi:10.1103/PhysRevB.102.174432.